arXiv:1612.00070v1 [astro-ph.SR] 30 Nov 2016

Rotation Periods of Wide Binaries in the Kepler Field

K.A.Janes

Astronomy Department, Boston University, Boston, MA 02215

Received _____; accepted _____

ABSTRACT

In a search of proper motion catalogs for common proper motion stars in the field of the Kepler spacecraft I identified 93 likely binary systems. A comparison of their rotation periods is a test of the gyrochronology concept. To find their periods I calculated the autocorrelation function of the Kepler mission photometry for each star. In most systems **for which good periods can be found**, the cooler star has a longer period than the hotter component in general agreement with models. **However,** there is a wide range in the gradients of lines connecting binary pairs in a period-color diagram. Furthermore, near the solar color, only a few stars have longer periods than the Sun, suggesting that they, and their cooler companions are not much older than the Sun. In addition, there is an apparent gap at intermediate periods in the period distribution of the late K and early M stars. Either **star formation in this direction has been variable, or** stars evolve in period at a non-uniform rate, or some stars evolve more rapidly than others at the same mass. Finally, using the autocorrelation function as a measure of the activity level, I found that while the F, G and early K stars become less active as their periods increase, there is no correlation between period and activity for the mid K to early M stars.

Subject headings: binaries: visual – proper motions – stars: activity – stars: late-type – stars: rotations – stars: solar-type

1. Introduction

It is by now well-established that stars with convective envelopes spin down as they age. Since the much-cited paper by Skumanich (1972) showing that solar-type stars follow an approximate $t^{1/2}$ relation for rotation period, a great deal of effort has been made to understand the underlying physical mechanisms and to derive a quantitative calibration valid for all cool, convective stars. For some recent discussions of stellar activity and stellar rotations, see Barnes (2010), Barnes & Kim (2010) and Reinhold, et al. (2013). The Sun and stars in young open clusters have been used as calibrators for the age-period-color relation (e.g., Meibom, et al. 2015), but it has been more difficult to find suitable calibrating stars to probe the rotations of older stars, particularly ones of later spectral types, (but see Mamajek & Hillenbrand 2008; Epstein & Pinsonneault 2014).

Efforts to provide a theoretical framework for stellar spin-down include Kawaler (1988), Barnes (2007) and Barnes & Kim (2010). The key parameter is the convective turnover timescale (Noyes, et al. 1984), a quantity not directly observable, that drives the magnetic activity level, which in turn controls the stellar wind that carries away angular momentum. Epstein & Pinsonneault (2014) have used a combination of models plus data from the open cluster M37 and binary stars to show that differential rotation and (in stars less than 0.6 $M_{\odot}$) the initial rotation rates are the limiting factors in the age precision of older stars.

The Kepler mission to search for exoplanets (Borucki, et al. 2011) has for the first time provided the observational material needed to extend the calibation of the age-rotation period-spectral type relation to older and cooler stars. Meibom, et al. (2011, 2015) have used Kepler data to calculate periods of a number of stars in the one Gyr cluster, NGC 6811, and the 2.5 Gyr cluster, NGC 6819. A much older cluster in the Kepler field, NGC 6791, is too distant to be useful for rotational measurements of the main sequence stars, but in the extended Kepler Mission (the "K2 Mission") the 4.0 Gyr cluster, M67, was observed,

and Barnes, et al. (2016) have derived periods for some of the cluster stars. However, all of these clusters are relatively distant, so cluster stars later than early K spectral type are too faint for Kepler. Angus, et al. (2015) used rotation periods of Kepler stars as well as cluster stars and other stars with known ages to derive a period-age-color relation of the form $P = aA^n(B - V - c)^b$, where A is the age of a star in Myr and a, b, and n are constants. They found however that some stars exhibited large deviations from the mean relation.

Mamajek & Hillenbrand (2008), compared the rotation periods of the components of a small sample of visual double stars; while the actual ages of the binary systems may not be known, their components can be expected to have the same age. Donahue (1998) had earlier applied the same idea to compare the chromospheric ages of visual binary star components. The Kepler mission has now made it possible to expand on the Mamajek and Hillebrand and Donahue ideas and fill in the gaps in the age-color-period relation with the help of binary stars. In the Kepler field, there should be a considerable number of common proper motion (CPM) stars, stars moving through space together; their components presumably have a common, if unknown, age. Deacon, et al. (2016) searched the Kepler field for wide binaries in the Kepler field, to learn whether wide multiplicity can affect planet occurrence. They found a number of likely binaries but only briefly considered thw question of gyrochronology. The aim of this project is to identify likely CPM stars in the Kepler field and use them to explore the existing age and spectral-type calibrations.

Section 2 is a description of the search process to find candidate CPM pairs and section 3 presents a confirmation of their binary nature from photometric data. The procedure for finding rotation periods from the Kepler photometry is the topic of section 4 and section 5 is a discussion of the period distribution of proper motion pairs.

2. Proper Motions

There are at least 6 proper motion catalogs covering stars in the Kepler field that might be of help to identify CPM stars in this region: The USNO-B catalog (Monet, et al. 2003), the UCAC-4 catalog (Zacharias, et al. 2013), the URAT-1 catalog (Zacharias, et al. 2015), the Hipparcos/Tycho catalogs (specifically the Tycho-2 catalog) (Høg, et al. 2000), the PPMXL catalog (Roeser, et al. 2010), and the Deacon, et al. (2016) study mentioned in the introduction that specifically targeted proper motions in the Kepler field. Although these catalogs are not fully independent of one another, and have a substantial overlap in the sources of positions from various epochs, there is nevertheless a considerable range in their completeness, magnitude coverage, astrometric and photometric precision and other characteristics.

To manage this heterogeneous set of data, I downloaded the data from the first five of the catalogs from the VizieR online database (vizier.u-strasbg.fr/viz-bin/VizieR). for an 8-degree radius field centered at $RA = 19^h22^m40^s, Dec = 44^d30'00"$, which covers the entire Kepler field of view. I also downloaded the complete Deacon, et al. (2016) catalog which covers approximately the same field.

Together, these catalogs include several million stars, but only 206150 stars were observed by Kepler. After downloading the positions, physical properties and photometry from the MAST data archive (archive.stsci.edu/kepler/), for all the stars observed by Kepler, I merged these data together with a revised set of effective temperatures and gravities for the Kepler list by Huber, et al. (2014). I then cross-referenced the merged MAST plus Huber, et al. (2014) data with all six catalogs to get a complete list of proper motions, photometry and other information for the Kepler targets. To match stars from any two of the 7 lists, including the Kepler target list, the positions must match within 2 arcseconds and the brightnesses must match within one magnitude. Although they are

on somewhat different photometric systems, each of the catalogs includes a red magnitude reasonably close to the SDSS r filter.

While the tabulated proper motion uncertainties in these catalogs are typically a few milliarcseconds per year, the actual proper motion *differences* from one catalog to the other are often substantially larger. For that reason, I did not use the published proper motion uncertainties, except for those in the Tycho catalog, in the following analysis unless the published uncertainty is larger than 10 msec/yr; in such cases, I disregarded that proper motion value altogether.

Most of the stars with Kepler photometry match up with entries in more than one proper motion catalog; some selection process is necessary to create a merged list of proper motions. The Tycho proper motions are presumably the most reliable, so if there are Tycho values for a star, I chose to use them, including the published Tycho uncertainties. For the fainter stars, I took the mean of the available proper motion values, giving double weight to the Deacon catalog, because it is based on a combination of modern CCD photometry and several earlier catalogs. The Tycho 2 stars are all brighter than about r = 13 and the Deacon, et al. (2016) catalog contains only stars fainter than r = 14.5. If there were three or more measurements and if one of the values differs by more than 25 msec/yr from the mean of the others, I tossed that value out. The resulting merged proper motions for the Kepler stars represent a compromise of the available data; for estimates of the uncertainties I simply took the standard deviation of the individual proper motion values.

The goal is to search for pairs of stars that appear to be moving together through space, that is to say, stars with a common proper motion. The typical proper motions of stars in this direction in the galaxy are close to zero, so for example, the mean proper motions of stars in the Tycho catalog are -0.4 and -3.1 milliarcseconds per year in RA and Dec respectively with dispersions of 9.7 and 14.8 milliarcsec per year. This means that

for two stars to be reliably identified as likely CPM pairs their proper motions must be substantial. But stars with large proper motions tend to be nearby, mostly low-luminosity dwarfs; in fact such stars are exactly the ones of interest for this project.

Given a target star in some direction in the galaxy, the number of stars within an angular distance, r_c, of the target is $\frac{1}{2}\pi r_c^2 \rho(b)$, where $\rho(b)$ is the star density at galactic latitude b. (The factor 1/2 accounts for the fact that for each target star, the search for companions proceeded only in the leading direction toward increasing RA - stars in the trailing direction would already have been searched.) In general, almost all stars are unrelated to the target star. The probability that a target star randomly has an *unrelated* companion with a proper motion, μ within some range, $\delta(\mu)$, of the target proper motion is $\sum N(\mu)/N_t$, where $N(\mu)$ is the density of stars in proper motion space at μ and N_t is the total number of stars in the particular sample. The summation is taken over the proper motion range $\pm\delta(\mu)$, the proper motion difference between the target star and its possible companion.

The total probability of finding an unrelated star near a target star is just the product of the factors:

$$P(\mu) = \rho(b)\pi r_c^2 \frac{\sum_{-\delta(\mu)}^{+\delta(\mu)} [N(\mu)]}{2N_t} \quad (1)$$

So given a target star, the angular separation and the proper motion difference between the two stars can be used in the above relation to get the probability that this combination could occur by accident.

Several additional constraints on possible companions are needed:

1) I limited the search radius to the range, $6.0 \leq r_c \leq 600$ *arcsec*. Although stars with a small separation are more likely to be binaries than wider pairs, blended images are a significant problem both for the measured proper motions and for the Kepler photometry.

2) The total proper motion of each star must be greater than 5 times the total proper motion uncertainty, which typically is of the order of 3 mas yr^{-1}; for stars in the merged list with no calculated uncertainty, I assumed an uncertainty twice that value.

3) For the proper motion search range, $\delta(\mu)$, around the target star, I used the lesser of the actual proper motion difference between the target and its possible companion or 5 mas yr^{-1}.

4) The total proper motion difference between the two stars must be less than 10% of the sum of their total proper motions.

5) In evaluating Equation 1, I took the number of stars brighter than the fainter of the two candidate stars as the value for N_T.

Using the constraints described above and the additional condition to consider only pairs with a probability, $P(\mu) < 0.001$ that they could be an accidental pair, a search of the working proper motion list yields 102 pairs of stars. As a test of the selection criteria, I repeated the search by successively adding and subtracting 20 arcminutes to the declination of each star before checking for matches to the target stars. These tests yielded 19 pairs when the declinations were shifted northward and 13 stars with a southward shift. Thus, as many as 15% of the pairs in the original search could be accidental pairs, but as shown in the next section photometric considerations lead to the elimination of additional stars.

Twelve of the candidate CPM stars are listed in the MAST archive as "Kepler Objects of Interest" (KOIs). Two stars have confirmed planetary systems - K06678383 (Kepler-104,b,c,d) and K12068975 (Kepler-197 b,c,d,e). and three more stars are listed as having candidate planets - K08845205, K09579208 and K11098013. Six stars are listed as "false positives" - K07013635, K07582691, K07885518, K07885570, K09762514, and K09762519. Three stars (K07885570, K09762519 and K06678383) are also listed in the

Villanova eclipsing binary catalog (Kirk, et al. 2016).

3. Photometry

The MAST data archive includes data for the Kepler stars on several photometric systems as well as photometrically derived effective temperatures, but many stars are missing values in one or more colors, in particular, the B and V magnitudes. However, the Kepler index g_{KIC}, which closely approximates the SDSS g index, and the 2-MASS K_s index are available in the archive for all but a few of the CPM stars. Furthermore, the color index, $(g_{KIC} - K_s)$, has good sensitivity to stellar temperature over a wide range of spectral types and is widely available in various stellar archives. In the following, I will refer to these indices as "g" and "$(g - K)$" respectively.

If indeed both members of a suspected CPM pair are main sequence stars at the same distance, then the magnitude difference between the two stars and their color index difference should be strongly correlated. The correlation may not be a simple one: the main sequence is not linear; some of the more massive stars may be evolved; some of the youngest, low-mass stars may not have reached the main sequence; or one or the other of the two stars may itself be multiple. Nevertheless, there is a well-defined correlation between the $(g - K)$ color differences and differences in the g magnitudes for most of the CPM candidates as shown in Figure 1a. The regression line in Figure 1a has the form $\Delta g = 1.890\Delta(g - K) + 0.079$. In contrast, there is no correlation between color and magnitude differences for stars in the two false positive tests (offsets North and South) added together (Figure 1b).

Three stars in the initial sample do not have g or K magnitudes, and their photometric data are incomplete in other respects as well. Six more pairs in Figure 1a, including one

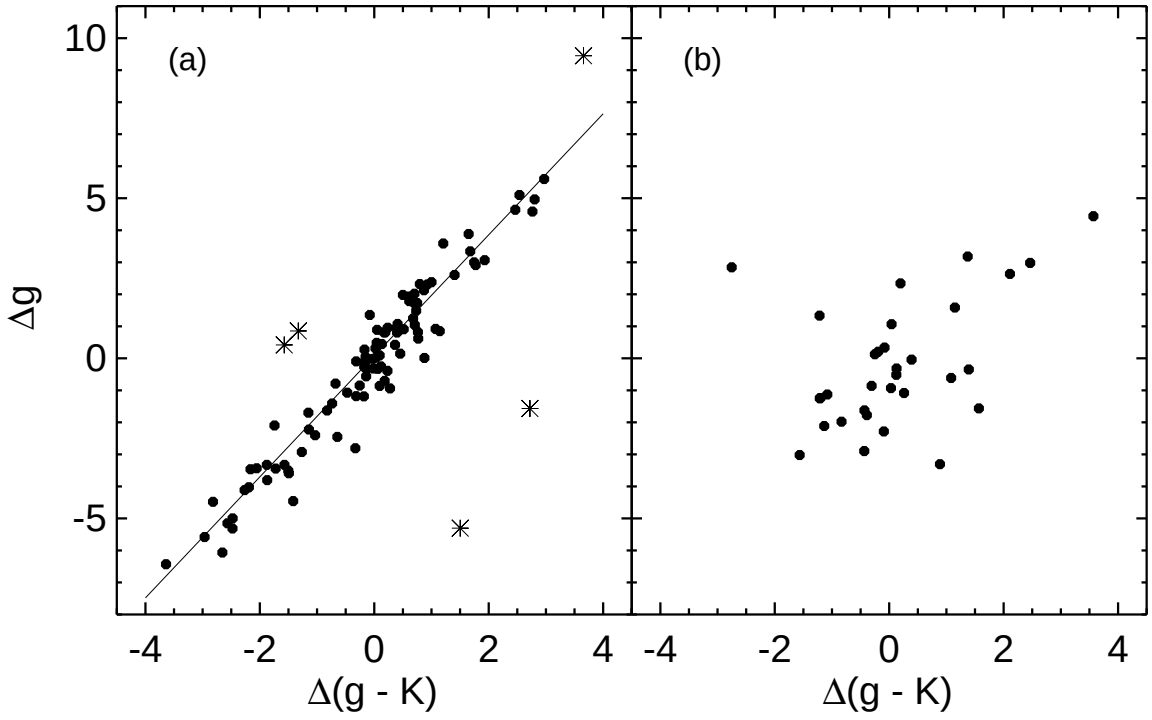

Fig. 1.— A comparison of the magnitude differences, Δg, vs the color index differences, $\Delta(g-K)$. (a) Candidate CPM pairs. (b) The two sets of false positives (created by adding or subtracting 20 arcmin to each target star before searching for companions). The asterisks in Figure 1a represent stars with photometry incompatible with being main-sequence common proper motion pairs. The regression line has the form $\Delta g = 1.890\Delta(g-K) + 0.079$.

outside the plotted area, are obvious outliers. They are either not physically related, or one of the components may be an evolved star. Several others are early-type stars, outside the range of interest for this project. I have rejected both components of these nine pairs from the CPM list. For completeness, they are presented in Table 1, which lists their KIC numbers, proper motions and uncertainties, angular separation, g magnitude and $(g - K)$ color index.

Several stars in the candidate list have Kepler gravities consistent with being evolved stars. Indeed two stars with gravities typical of red giants are among the outliers in Figure 1. Three other possibly low-gravity stars have gravities characteristic of supergiants, but their proper motions, their positions in Figure 1 and, in two cases (K08888543 and K08006740) their light curves, indicate that they are completely normal dwarfs. The third star of this group (K11503111) has an anomalous light curve, suggesting some instrumental problem. The Huber, et al. (2014) gravities for 4 additional stars (K09468112, k08098181, K02992960, K02992956) indicate that they may be slightly evolved, but they also fit near the fiducial line in Figure 1. The first of these four stars has properties consistent with its partner, but the second star is a member of a close pair with mutually compromised light curves. The last two of these form a binary pair with almost identical properties, including their periods; they could be slightly evolved. Since this group of stars listed with low gravities in Huber, et al. (2014) fit the regression line in Figure 1 they remain in the list for now. The remaining stars have gravities consistent with their locations on the main sequence.

The final list of candidate CPM stars includes 93 pairs; they are presented in Table 2. The first column in Table 2 is a running pair number; column (2) represents the KIC number from the Kepler input catalog; the next four columns represent the RA and Dec proper motions and their uncertainties, column (7) is the angular separation of the two

components, column (8) is an index of the relative probability that it is a common proper motion pair on a scale where a 99 indicates $P(\mu) = 0.00099$ (see Equation 1), column (9) is the g magnitude, and column (10) is the $g - K$ color. The remaining columns will be described in the following section.

Because most of the stars that satisfy the present criteria are relatively nearby, they should be expected to have low interstellar reddening. In any case, since the two components presumably lie at the same distance, the reddening would be expected to be the same, and so will not affect Figure 1.

The Kepler data archive does include reddening values for many of the Kepler targets, so to correct the photometry for the effects of reddening, I corrected each pair by the average reddening of the two stars.. In cases where one (or both) of the members did not have a reddening value, I assigned a value of $E(B - V) = 0.06$ (the mean value of the stars in this sample with reddening values), before calculating the average value for that pair. To correct the $(g - K)$ and g indices, I applied the extinction coefficients described by Yuan, et al. (2013). With help of their Table 2, I found that $A(g) = 3.30E(B - V)$ and $E(g - K) = 2.99E(B - V)$.

4. Rotation Periods

The Kepler PDC-MAP long-cadence data for each star (obtained from MAST) consists of a nearly continuous series of brightness measures with a cadence of about 30 minutes ($\sim$0.0204 days), covering a period of 4 years. The data for each approximately 90-day period, or "quarter," were processed separately, so there are differences in photometric zero-points and other parameters from quarter to quarter. As described in the archive, each quarter's data have been independently processed to remove most instrumental artifacts,

Table 1. Stars with Similar Motions Rejected as Common Proper Motion Pairs

CPM pair	KIC	μ_α msec/yr	e_{μ_α} msec/yr	μ_δ msec/yr	e_{μ_δ} msec/yr	Sep arcsec	g mag	$(g-K)$ mag
11	7940959	-28.4	0.8	-34.9	0.9	160.2	8.482	3.481
11	7941056	-23.9	1.2	-32.2	1.9	160.2	13.787	2.200
28	9942231	-6.9	0.0	89.9	0.0	58.7	0.000	0.000
28	9942242	-5.8	1.3	86.1	1.3	58.7	17.597	4.460
30	11603064	-8.2	1.3	-17.4	1.3	94.2	8.437	2.595
30	11603098	-7.6	1.5	-20.6	1.5	94.2	10.003	0.513
41	12645102	-5.8	2.5	-21.8	2.2	54.7	12.806	1.309
41	12645107	-7.2	2.7	-18.6	2.5	54.7	11.951	2.303
44	12254819	21.4	0.0	62.6	0.0	7.9	0.000	0.000
44	12254821	20.4	0.7	68.5	4.5	7.9	13.116	3.345
48	7816381	-6.2	1.6	45.8	1.7	14.3	17.688	3.212
48	7816387	-8.7	1.3	47.4	1.9	14.3	13.153	1.449
56	8557567	-76.5	0.0	-132.8	0.0	302.5	18.512	4.799
56	8557784	-71.3	1.0	-130.0	1.0	302.5	9.062	1.628
75	11822514	25.0	1.3	44.6	1.7	29.4	17.528	4.926
75	11822535	23.0	1.3	46.4	1.0	29.4	14.455	-0.913
83	11774619	-28.0	0.8	-31.7	1.6	37.6	16.567	2.780
83	11774639	-24.5	1.0	-26.8	0.8	37.6	16.148	4.758

Table 2. Selected Common Proper Motion Stars in the Kepler Field

CPM pair	KIC	μ_α	e_{μ_α}	μ_δ	e_{μ_δ}	Sep	I_{RP}	g	$g-K$	Period	e_{Period}	V	σV	N_{qtrs}	Type
		msec/yr	msec/yr	msec/yr	msec/yr	arcsec		mag	mag	days	days	ppm	ppm		
(1)	(2)	(3)	(4)	(5)	(6)	(7)	(8)	(9)	(10)	(11)	(12)	(13)	(14)	(15)	(16)
1	7090649	16.1	0.6	10.8	2.5	9.3	99	11.976	2.277	8.27	0.11	6705.7	5.52	17	P
1	7090654	17.6	1.1	13.8	1.1	9.3	99	10.249	1.528	1.98	0.00	2578.3	52.0	17	P
2	7659402	28.5	0.5	8.9	1.1	29.0	56	16.708	4.593	19.66	0.28	801.1	8.2	4	A
2	7659417	27.2	0.9	7.9	1.5	29.0	56	17.559	4.848	16.31	0.53	44.8	5.0	17	P
3	7582687	-26.5	1.5	-25.0	1.0	21.8	93	13.066	2.172	14.07	1.94	46.1	2.4	17	P
3	7582691	-23.4	3.0	-23.8	0.6	21.8	93	16.499	4.227	24.54	0.12	642.7	5.8	14	A

Note. — Table 2 is published in its entirety in the electronic edition of the *Astronomical Journal*. A portion is shown here for guidance regarding its form and content.

while hopefully having only a minimal effect on the astrophysical phenomena.

Assuming that the ubiquitous brightness variations of cool main sequence stars are the result of rotational migration of starspots across the visible hemisphere, it should be possible to identify the rotational period with standard time series analysis methods. Following McQuillan, et al. (2014) I computed the autocorrelation function (ACF) of each star's PDC-MAP lightcurve.

To compute the ACF, I began by subtracting the mean value of each quarter's measures and dividing by the quarterly rms value.

$$P(i,j) = \left[F(i,j) - \bar{F}(j)\right] / \sigma_{\bar{F}(j)}, \tag{2}$$

where $F(i,j)$ is the measured flux of observation i in quarter j, $\bar{F}(j)$ is the mean value of the data for quarter j and $\sigma_{F(j)}$ is the rms value of the zero mean values in quarter j. So $P(i,j)$ has a mean value of zero and unit variance separately in each quarter. But the variance of the original data, $F(i,j)$, will in general differ from quarter to quarter, as a result of both instrumental and astrophysical differences in the quarterly data sets. In particular, because of the small scale difference from quarter to quarter and because of differences in the variance there will be (generally) slight scale differences in the distribution of measurement uncertainties from one quarter to the next. Figure 2 shows one of the more noticeable cases of this phenomenon. The upper diagram shows the 17 quarters of data with the quarterly mean values subtracted; in the lower figure the data have also been divided by the quarterly rms values. The assumption here is that these inconsistencies will be immaterial to finding periods.

The ACF, A(k), can be defined as

$$A(k) = \frac{1}{\sum_j \left[n_{jk} - k\right]} \sum_j \left\{ \sum_i \left[P(i,j)P(i+k,j)\right] \right\}, \tag{3}$$

where k is called the *lag*, measured as multiples of the 0.0204 day observing cadence. The

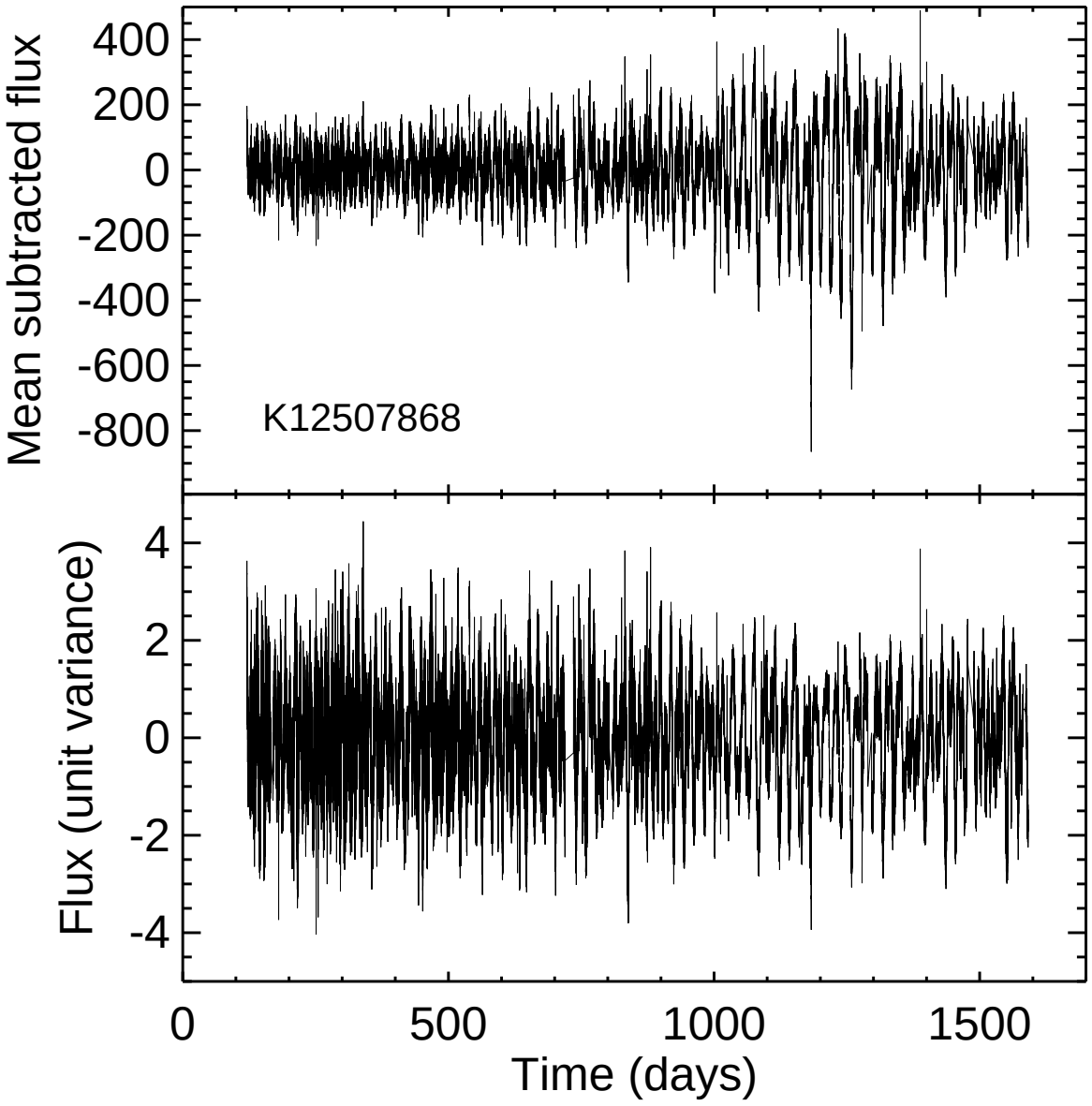

Fig. 2.— Star K12507868. The upper figure shows the 17 quarters of PDC-MAP data with the quarterly mean values subtracted. In the lower figure, the quarterly data values have also been normalized to unit variance by dividing by the quarterly RMS value.

number of useful measures in each quarter at lag, k, is n_{jk}. Any periodic variations in the measured brightness of the star (possibly the rotation period) will generate an ACF with a series of peaks with lag values at multiples of the period. As Equation 3 shows, the final value of $A(k)$ is the sum of the correlations over all data segments and can vary between plus and minus one.

By calculating the ACF in this way, three problems are overcome. First, the Kepler quarterly datasets are somewhat independent of one another, with slightly different scale factors and independent calibations. Second there are gaps of various lengths in the data; n_{jk} represents the actual number of measures for a particular star in quarter j. Finally, while the rotation periods are completely regular, the spot features, on which the measurements depend, change on time scales that may be shorter than a single rotation, and are rarely completely correlated over many rotations. So it is appropriate simply to add up a series of relatively short segments that each are more-or-less correlated over one or a few rotation periods.

Figures 3 - 6 illustrate the range of shapes taken by the ACF curves. Active stars with long-lived surface features exhibit regular patterns (Figure 3), athough it is not always certain what the true rotation period is (e.g., Figure 4). Less active stars may show hints of periodic variation (Figure 5), although the variations could instead be primarily instrumental in origin, particularly at large periods. Finally, some stars have more complex behaviour (Figure 6), and as mentioned above, several several stars are KOI's selected as possible planet hosts or eclipsing binaries.

Notwithstanding the smooth, repetitive patterns of Figures 3 and 4, There are in many cases large differences in the patterns from quarter to quarter. For example, Figure 7 illustrates the individual quarterly ACF patterns for star K12507868 (see Figure 4). There are considerable differences in the character of the variability from quarter to quarter; it

is only in the summation of $A(k)$ over several quarters that the dominant pattern (which presumably is the actual rotation period) becomes apparent. For that reason, the rotation periods of stars with measures over only a few quarters are often considerably less certain.

After calculating the ACF of a star, the next step is to find its period, or periods, by searching for peaks in the ACF. First I smoothed the ACF function by finding the maximum-likelihood cubic spline interpolation coefficents to fit a smooth curve through the ACF points. In Equation 2 the individual data points, $P(i, j)$, are defined by the original measures, with a cadence of approximately 30 minutes. I chose the spline knot points at multiples of 24 datapoints i.e. at multiples of about one-half day. Given a starting set of knot points, I used a simple Monte-Carlo process to find values for the spline coefficients that minimize the standard deviation between the actual data points and the calculated spline function. Figure 5 illustrates the fitting of a spline curve to a somewhat noisy, low-amplitude ACF.

The fitting program chose the peaks, i.e., the local maxima in the smoothed ACF, and the initial estimate of the rotation period was taken to be the mean of the separations between the identifiable peaks in the smoothed ACF. In some cases, after inspecting the individual ACF functions, I selected twice the initial period if there were alternating peak heights (see, e.g., Figure 4). There are also several stars with a pattern of peak heights repeating in groups of three with the third peak being the highest. For the period uncertainty, I took the standard deviation of the period measures.

The rotation periods and uncertainties are listed in columns 11 and 12 of Table 2 and the number of Kepler quarters used in the analysis are given in column 15. Stars with period uncertainties listed as 0.00 are all short period stars with uncertainties less than 0.01 day.

McQuillan, et al. (2014) did an autocorrelation analysis similar to the present one.

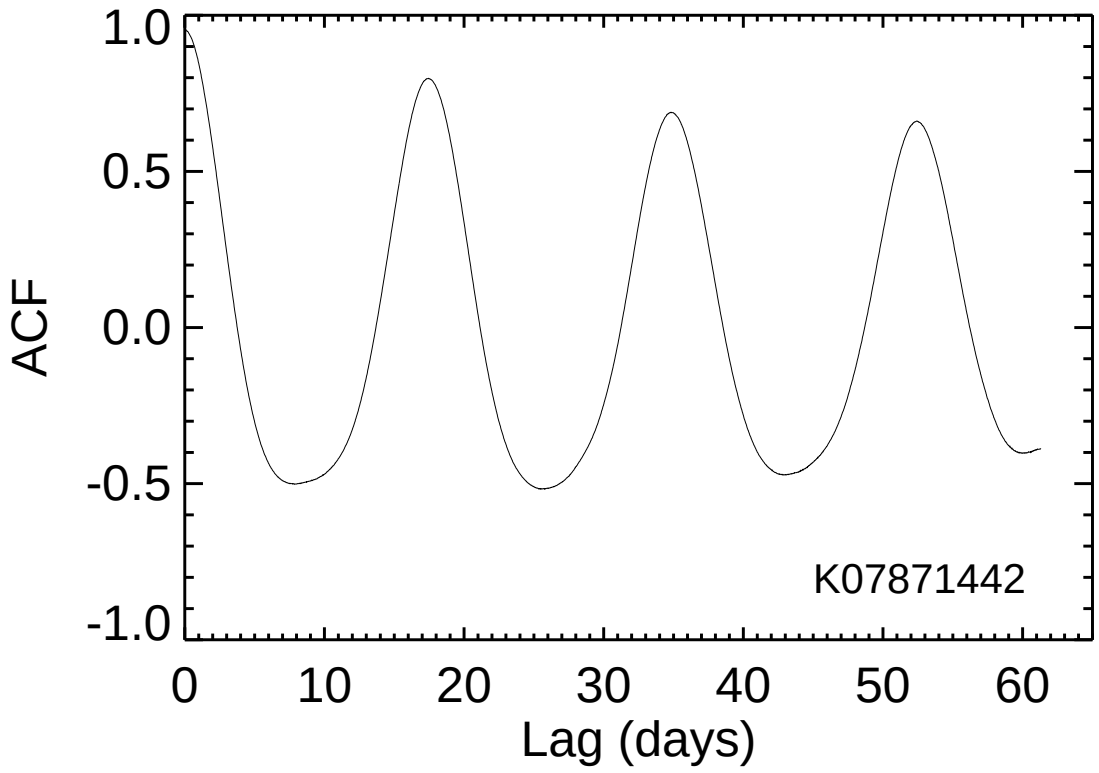

Fig. 3.— Star K07871442, an early M star with a well-defined ACF, indicating a period of 17.45 days. This curve covers 17 quarters of Kepler data.

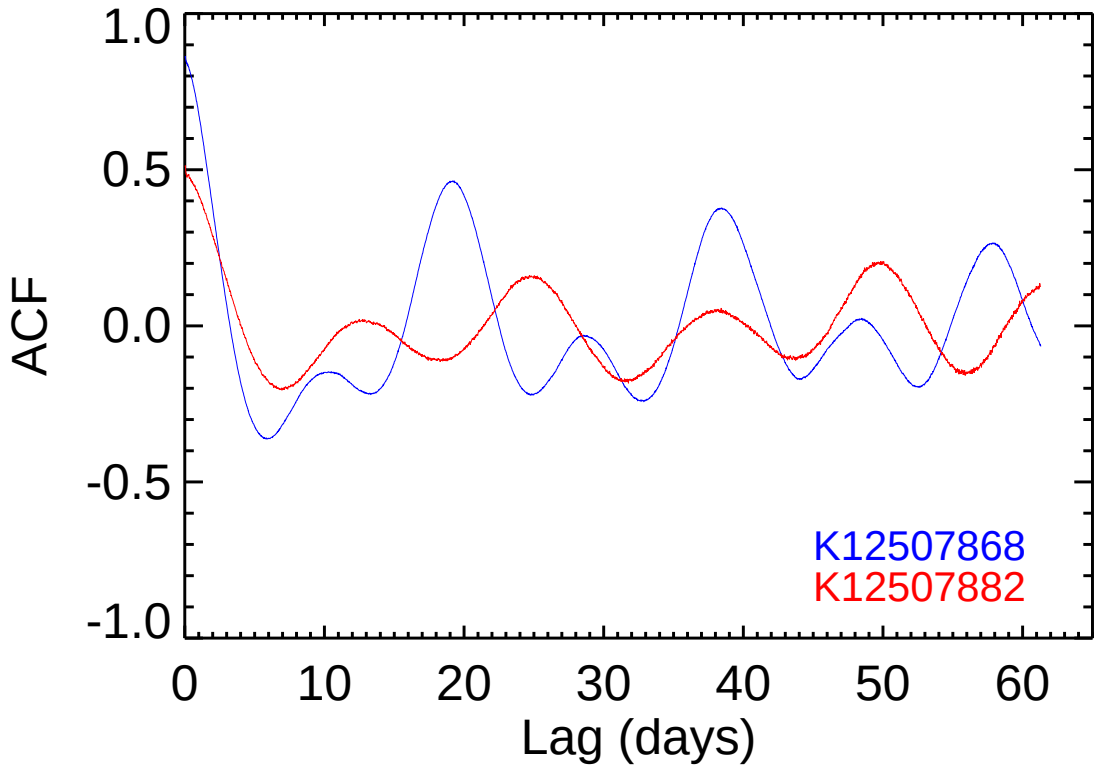

Fig. 4.— Two components of a CPM pair, K12507868 and K12507882, both of which have alternating peak heights. The periods derived here, 19.25 days and 24.82 days are in good agreement with the values found by McQuillan, et al. (2014).

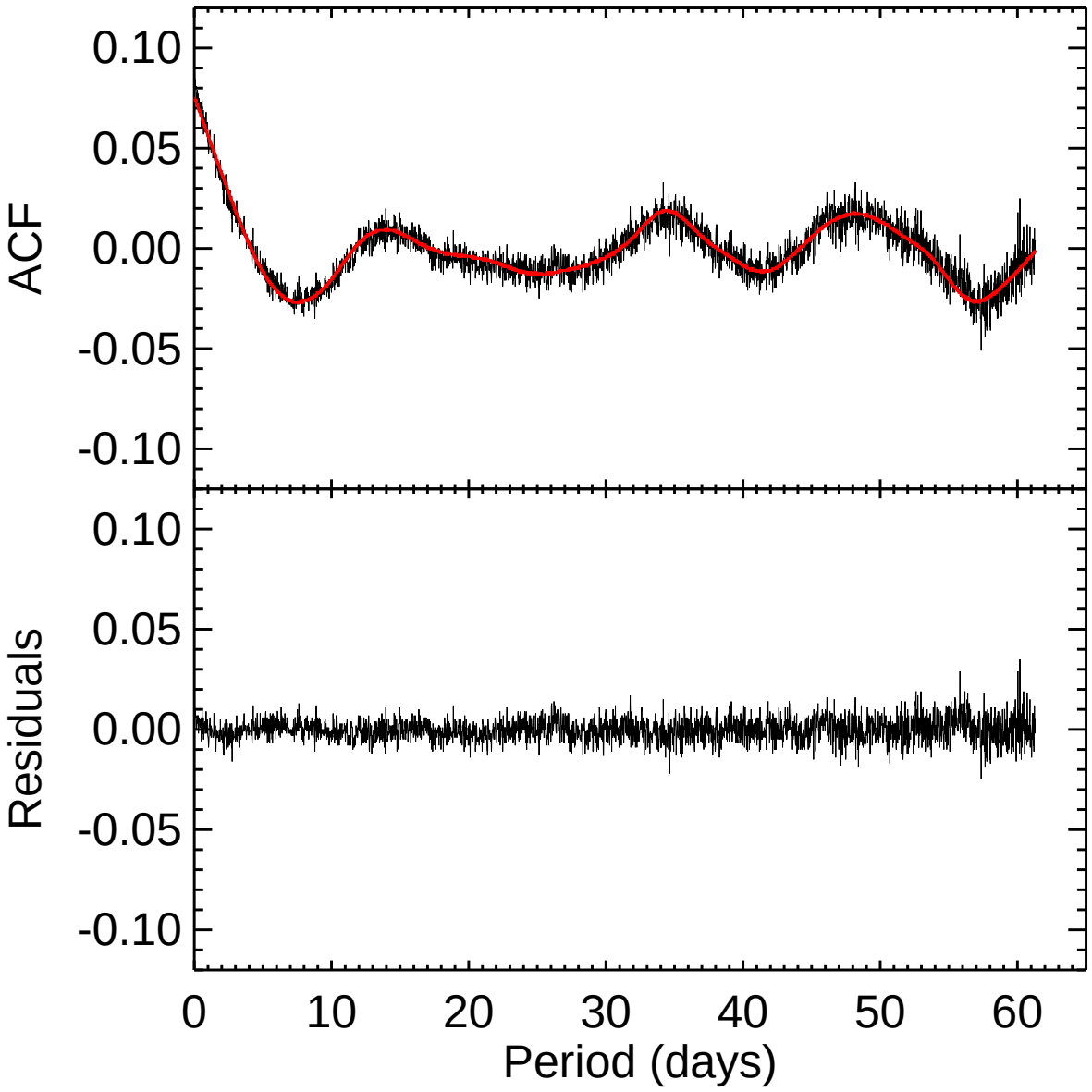

Fig. 5.— Star K09762514, which has a rather noisy, low-amplitude ACF, showing limited evidence for activity. The red curve in the upper figure is an illustration of the spline fitting to the ACF, with knot points at 2.5 day intervals. The best period found here is 16.08 days. McQuillan, et al. (2014) considered the period to be indeterminate, quoting a tentative value of 45.209 days. The lower curve shows the residuals between the data and the spline fit. The peak amplitude of the ACF is 9.3 ± 2.8 (ppm).

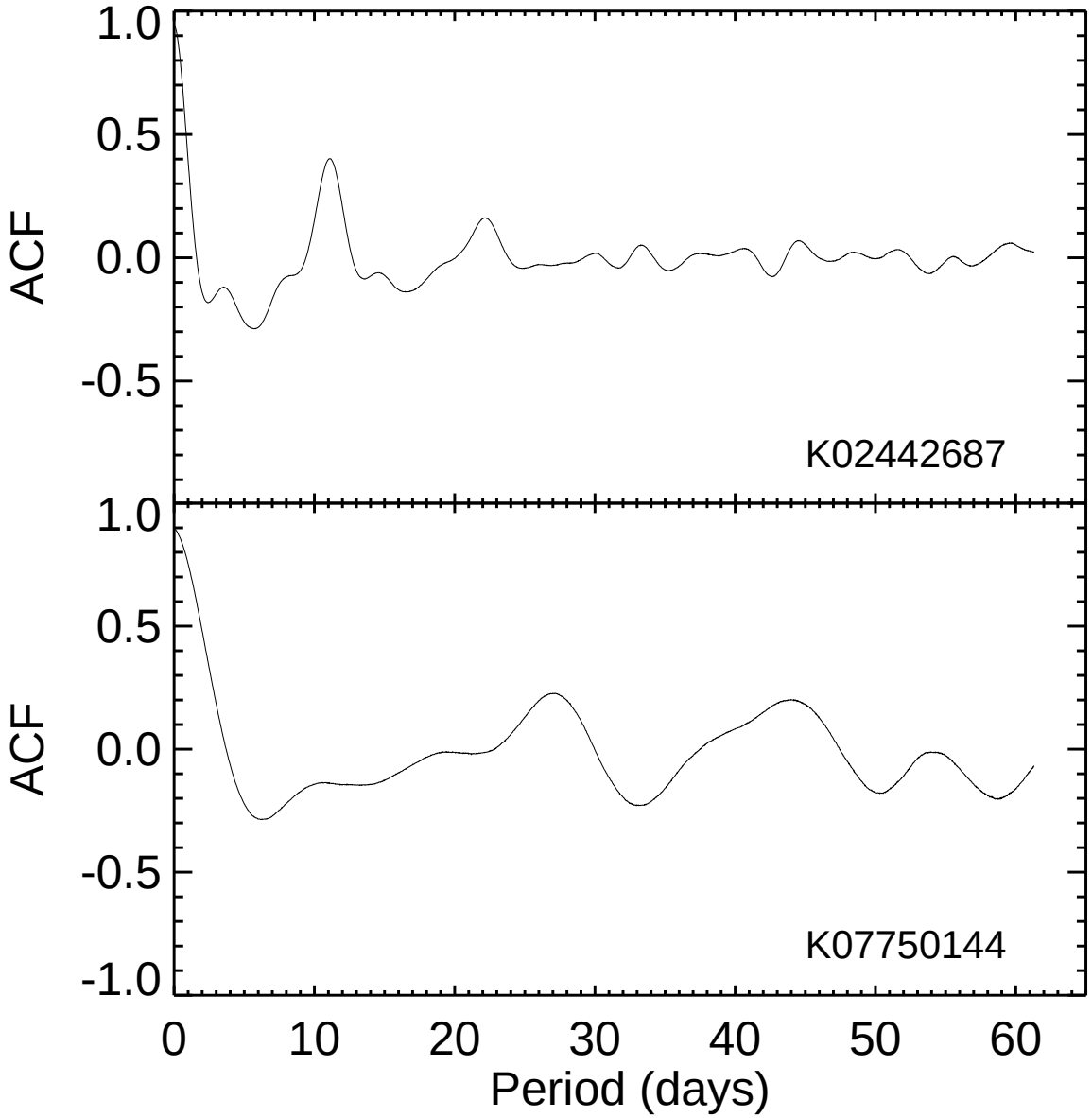

Fig. 6.— Two stars with somewhat complex ACF curves. K02442687 is an F star with a possible period of 10.98 days; its ACF curve is typical for the earlier spectral-type stars. K07750144 is a solar-type star with a possible period of 27.08 days. The former star is outside the temperature range searched by McQuillan, et al. (2014), but they found a period of 26.431 days for the latter.

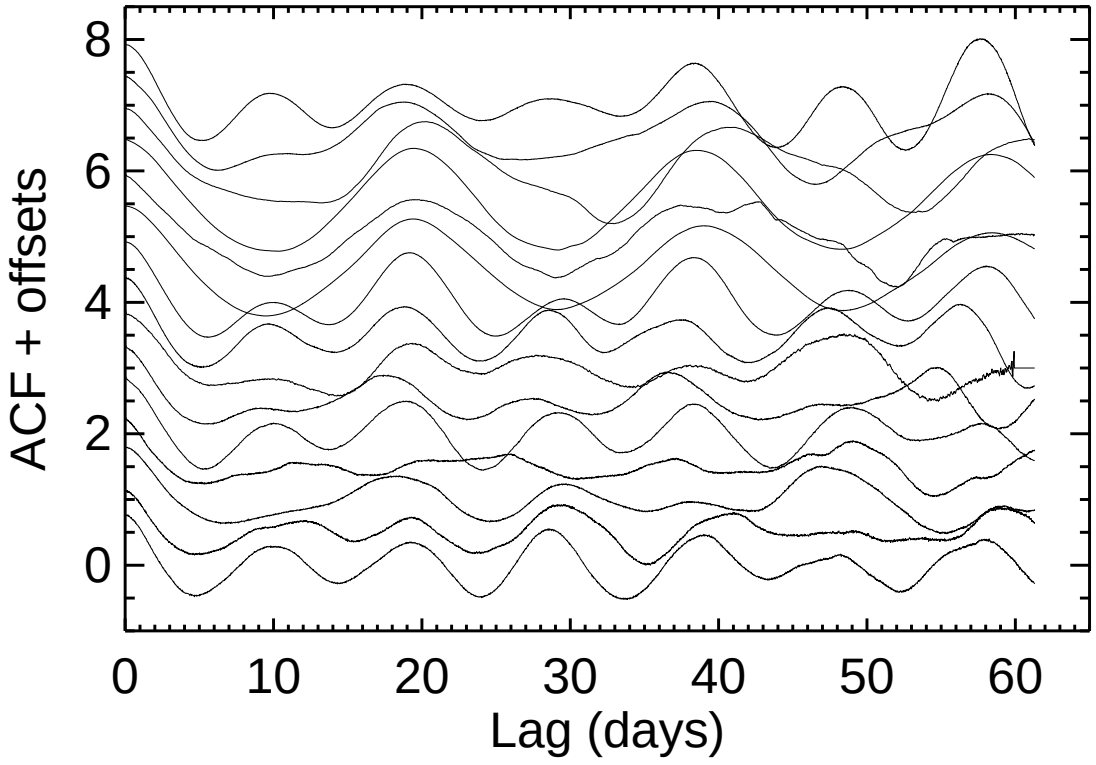

Fig. 7.— ACF curves quarter-by-quarter for star K12507868. Successive quarters are offset by factors of 0.5 for display purposes. The composite curve over all quarters is shown in Figure 4

After searching 133,030 main sequence Kepler stars for periods, they were able to calculate rotation periods for 34,030 stars. Their full sample included 120 of the 186 CPM stars in Table 2, but only 58 stars are in common between Table 2 and the 34,030 stars for which they found good periods. In addition to excluding known red giants, they rejected KOI stars, ones with no effective temperature or gravity measures, stars with $T_{eff} > 6500K$, and stars that were followed for fewer than 8 quarters. For the 58 stars in common to the two studies, the agreement is generally very good, even though there are some small differences in the procedures. Figure 8 shows the differences between the McQuillan, et al. values and the values in Table 2. There are eight stars for which their periods disagree by more than a little over one day. Star K10388259 has a very low amplitude and long period, so a difference of 4 days out of 48 is not surprising. For three more stars (K04544938, K04946401 and K10230145), the McQuillan, et al. periods are twice the values in Table 2 and for another star, the Table 2 value is twice the McQuillan, et al. period; either period is possible as the actual rotation period for these stars. The remaining three stars (K04931390, K10388283, and K11876220) all have two distinct, very regular, periods. I find 0.3 & 7.62 days, 2.74 & 38.82 days and 1.47 & 20.83 days respectively for these three stars. They are not included in the figure. For the remaining 50 stars, the difference is -0.05 ± 0.46 days.

4.1. Stellar Activity

The autocorrelation function (Equation 3) is normalized by the variance of the data, so by definition, the ACF at zero lag has a value of one. In the case of a function consisting purely of random noise, all other values of $A(k)$ would have a value of zero, within the noise level. But if a function has at least some degree of correlation at periods greater than the sampling period, $A(k)$ will vary with k depending on the functional form and the degree

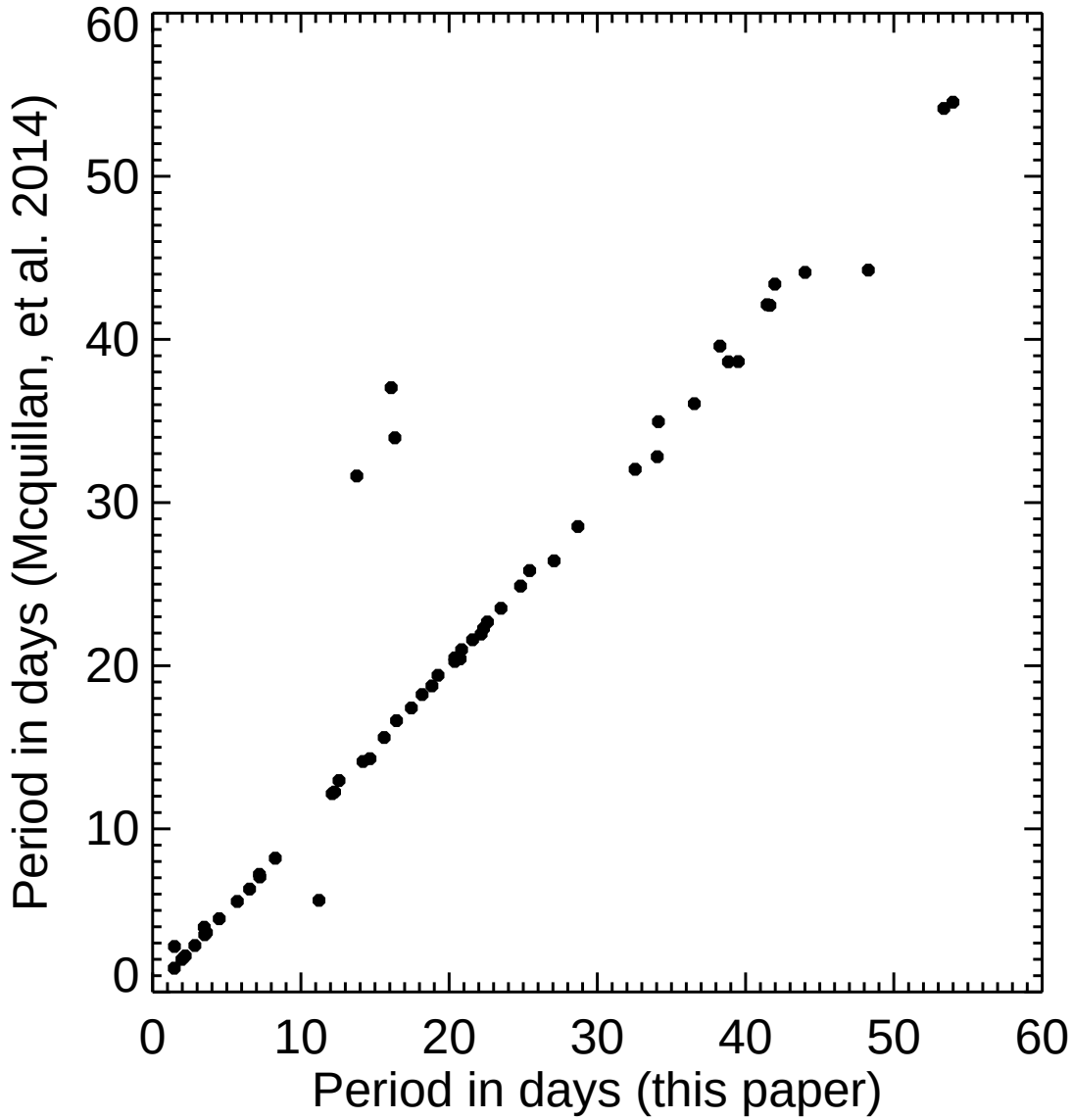

Fig. 8.— Comparison between the rotation periods in this paper and those of McQuillan, et al. (2014).

of the correlation. So the autocorrelation coefficient simply shows the degree to which the data are correlated at some particular value of k; when there are peaks in the ACF, they indicate the presence of a periodic phenomenon, which could be either instrumental or intrinsic to the star.

Some commonly used measures of the activity level of stars in the Kepler program are derived from the variance of the data, such as the range of variation between the 5th and 95 percentiles of variation (see Basri, et al. 2013, for example). But this definition does not distinguish between random noise and intrinsic variability. With the help of the ACF, it is possible separate the variance into its random and periodic fractions. The ACF value at a peak represents the correlated fraction of the variance at that period - so the product of the total variance and the ACF value at the peak can be used as a measure of the actual stellar variability:

$$V = 1000000 \frac{A_{max}}{n_q} \sum_j \sigma_{\bar{F}(j)}, \tag{4}$$

where A_{max} is the value of the ACF at the highest peak, n_q is the number of quarters this star was observed and $\sigma_{\bar{F}(j)}$ is the rms value of the zero mean of the data in quarter j, including both random noise and any intrinsic or instrumental signals as defined in Equation 2. The result is a fractional periodic amplitude in units of parts-per-million. For brighter stars A_{max} may be close to 1, that is the quantity V is dominated by the intrinsic variance of the data, and the purely random noise component is small. For stars that are almost constant, or for faint stars, A_{max} may be (sometimes much) less than one so V is less than the total variance of the data. To the extent that correlated instrumental (non-astrophysical) signals can be ignored, V is a measure of the intrinsic variations of the star. The uncertainty in V is just random component of the variance of the data; it is eqal to the standard deviation of the residuals of the cubic spline fit to the ACF curve (see, e.g. Figure 5). The variability measures, V, and σ_V are listed in columns 14 and 15 of Table 2.

Column 16 of Table 2 describes the visual appearance of the ACF. Stars with regular nearly equal peaks are labelled with a "P," (as in Figure 3), those with alternating peak heights (see Figure 4) are designated with an "A" and triple-peaked stars with a "T." The 31 stars with $V/\sigma_V < 5$ are designated as "I" (indeterminate) in Table 2. Those with indeterminate periods are either nearly constant or very faint or they were observed for only a few quarters. All but one of the indeterminate stars with $(g - K) < 3.5$ were observed for more than 10 quarters, but no reliable periods could be found; they are simply inactive. Nearly all of the cooler stars were observed for four or fewer quarters, and although some of them showed signs of variability, it was not possible to determine reliable periods. Another 14 stars (designated with a "C" in Table 2) exhibited various pecularities in their ACF curves; several of them have two distinct periods. Most of the stars in this group were close pairs with separations less than about 15 arcseconds and several of them interfere photometrically with one another. The C-type stars are not included in the analysis. The remaining 141 active stars, including 56 complete pairs, make up the primary sample for this analysis. They are variable presumably as a result of active regions moving across their surfaces as they rotate.

Figure 9 shows the relation between rotation period and the log of the activity index, V for all of the active stars. The upper diagram includes stars with $(g - K) < 3.0$ ($T_{eff} \sim 4750K$, spectral type K3) and the lower diagram shows cooler stars with $(g - K) > 3.0$. There is an expectation that as stars age, the level of activity decreases and the rotation period increases (see the Introduction). But as this figure shows, at every period there is more than a two order-of-magnitude variation in the activity level. The bluer stars do show a general declining trend in activity with increasing period in agreement with previous work. However, among the redder stars, except for a few of the shortest period stars which tend to have higher activity levels, there is no correlation between activity and rotation period between about 10 days and 50 days. Overall, the cooler stars have higher

activity levels than the hotter stars at every period.

5. Gyrochronology

The relationship between stellar ages, rotation periods and colors (or mass) for F, G, K, and M stars younger than about 600 Myr has been thoroughly studied using open clusters up to the age of the Hyades and Praesepe. Now, as described in the introduction, the age-period-color relation for F, G and early K stars has been extended to the Sun's age, with the help of open clusters observed by the Kepler mission. But because the clusters are all distant, the age-period-color relation for the cooler stars (beyond early K spectral type) is still mostly unknown. The present sample of common proper motion stars span the range of late-type main sequence stars from mid-F spectral type to early M stars.

Since a number of the stars in the present sample are missing B-V photometry, it was convenient in sections 3 and 4 to use (g-K) as the color index. But to permit comparison with previous work, I have taken photometric data compiled in the MAST to transform the (g-K) colors into (B-V). Figure 10 shows the relation between (g-K) and (B-V) for those stars in the CPM sample that have both colors. A simple quadratic least-squares solution to the data gives:

$$(B-V) = (-0.103 \pm 0.002) + (g-K)(0.424 \pm 0.000) - (0.028 \pm 0.006)(g-K)^2. \quad (5)$$

Figure 11 shows the period-color relation for the 56 active CPM pairs, with B-V values derived from equation 5. The solid lines in the figure connect the hotter star (blue symbol) of each pair with its cooler companion (red dot). Figure 12 is a companion figure showing all 141 active stars without the connecting lines.

For comparison, the Sun's position in these diagrams is shown with a dotted circle. For the age of the Sun, I took the recent meteorite value of Connelly, et al. (2012), 4.57

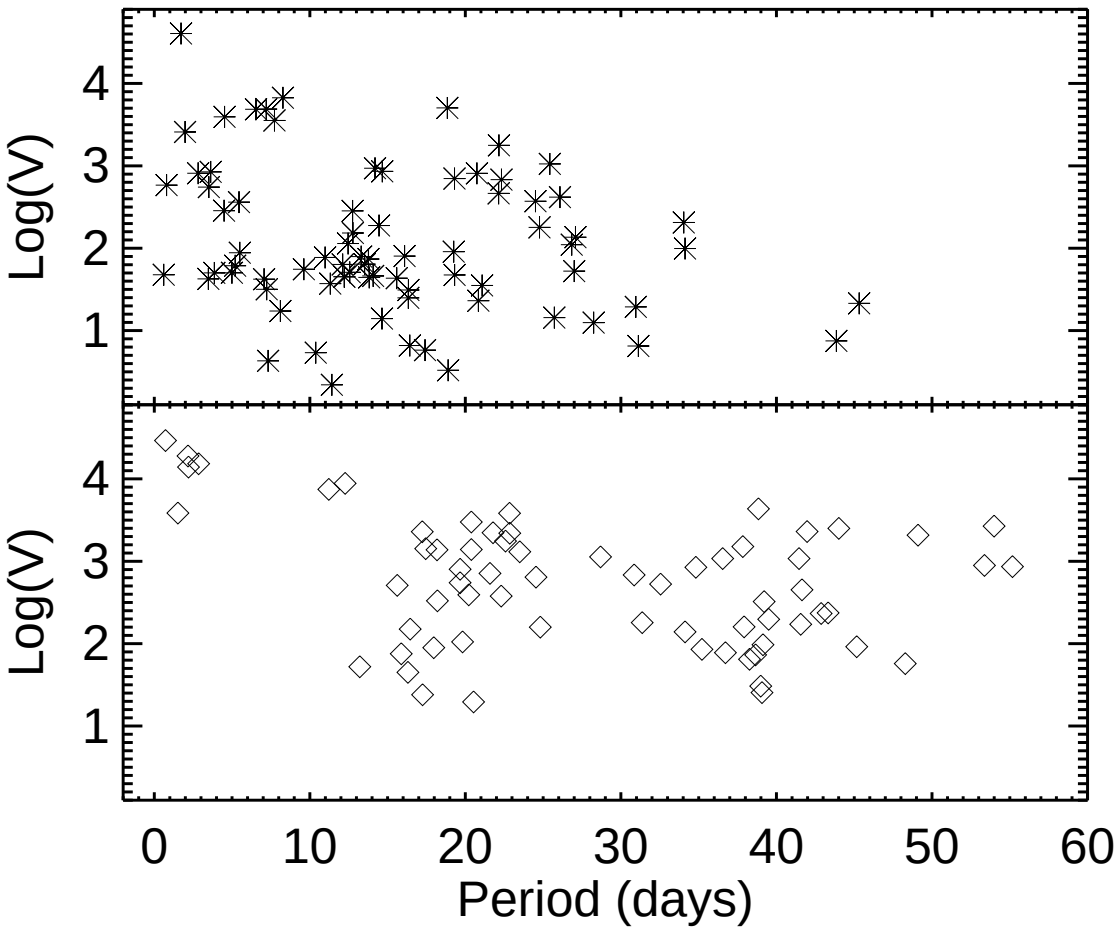

Fig. 9.— The rotation periods vs activity levels of all active stars in the CPM sample are shown. The asterisks (upper figure) represent stars with $(g - K) < 3.0$ and the diamonds (lower figure) are stars with $(g - K) > 3.0$. Stars labvelled "I" or "C" are not shown.

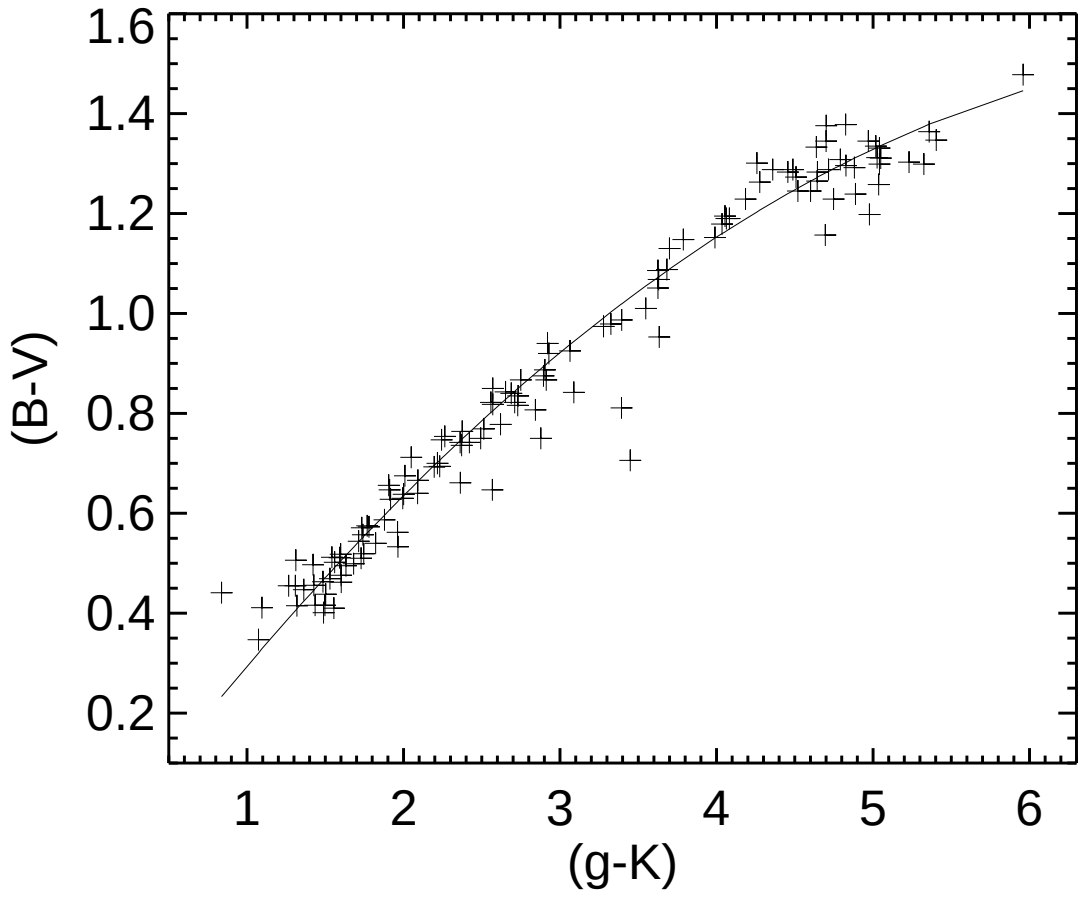

Fig. 10.— The (g-K) vs (B-V) color indices from the MAST archive for all stars in the present sample with tabulated colors. The photometry has been corrected for reddening using data from the archive. For stars without reddening values, I used $E(B-V) = 0.06$. The solid line is a simple quadratic least-squares fit of (g-K) to (B-V) after correcting for reddening (Equation 5).

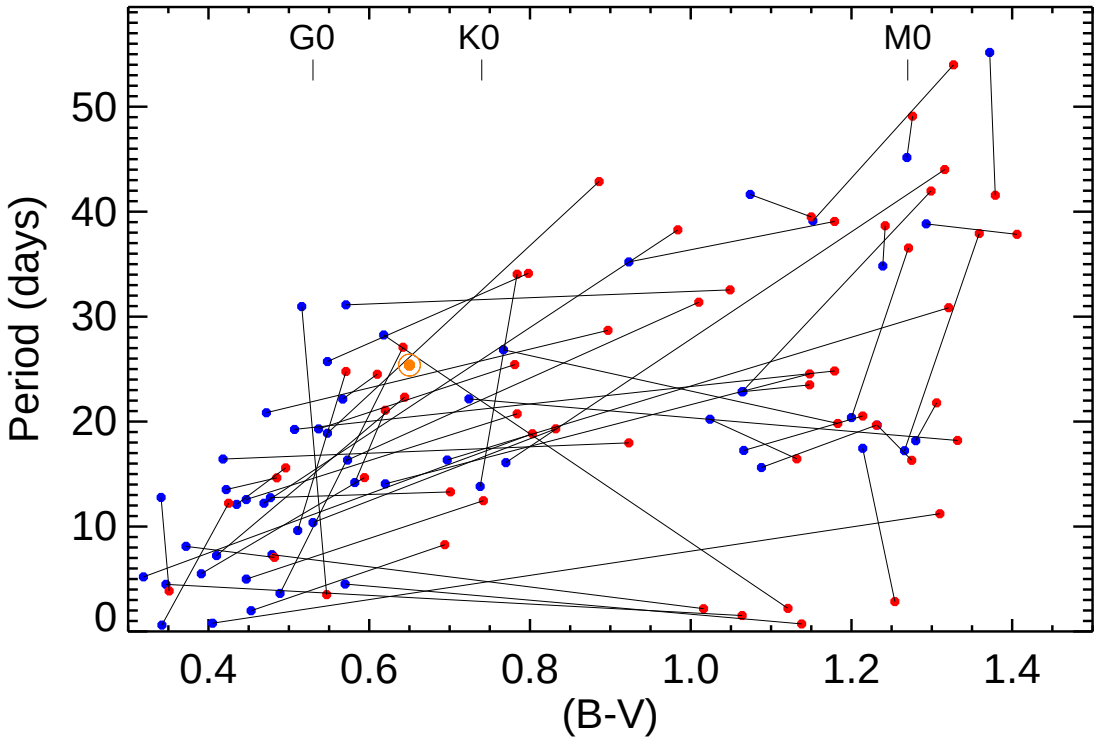

Fig. 11.— Period-color diagram for CPM pairs with two active components. The lines connect the hotter star of each pair (blue symbols) with the cooler star (red symbol). The (B-V) values are derived from Equation 5. The Sun's position is shown with a dotted circle. The approximate locations of selected spectral types from Table 5 of Kraus & Hillenbrand (2007) are also shown. **The blue component of one active pair (number 80) lies outside the diagram so that pair is not shown.**

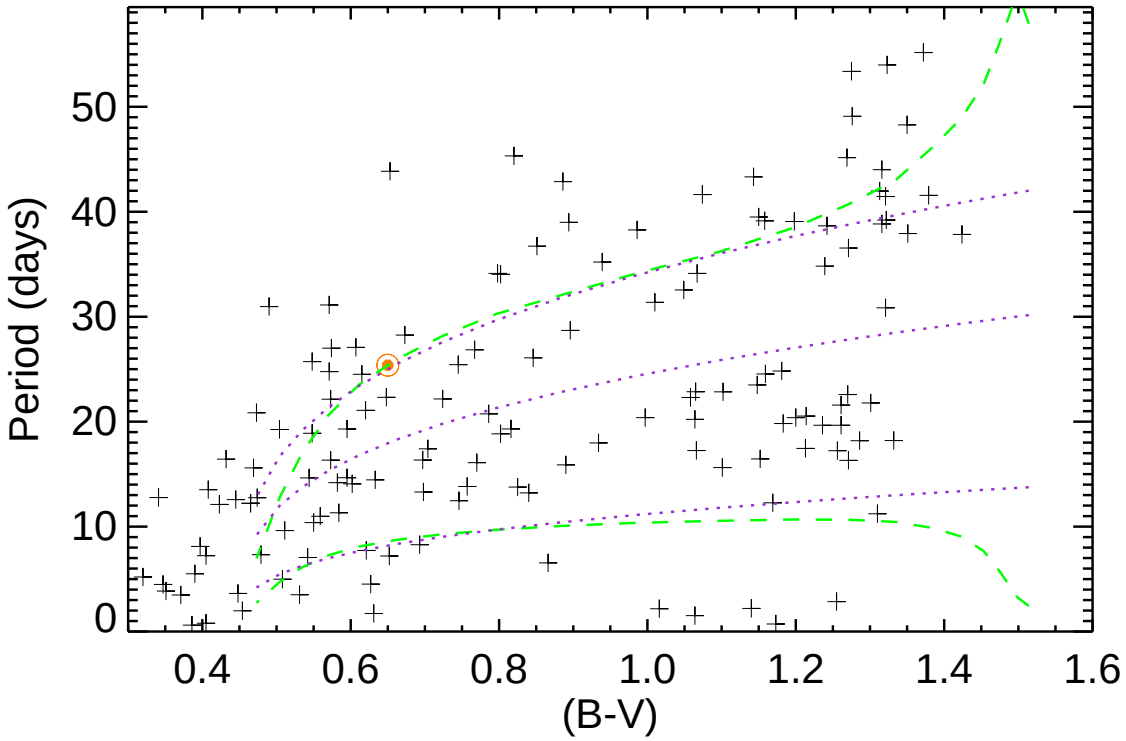

Fig. 12.— Period-color diagram for all active stars with reliable periods. The Sun's position is shown with a dotted circle. Period-color isochrones are shown for 4.57 Gyr, 2.5 Gyr and 600 Myr stars. The green lines are from Barnes (2010) and the purple lines are from Angus, et al. (2015). The upper two lines are the 4.57 gyr isochrones. The purple dotted line at intermediate periods represents a 2.5 Gyr isochrone from Angus, et al. (2015).

Gyr. Because of differential rotation, the Sun (presumably along with most of the other stars discussed in this paper) does not have a unique rotation period. I took the sidereal Carrington Rotation Period value of 25.38 days, which corresponds to the solar rotation at 30° latitude, the typical latitude of sunspots.

5.1. The period-color distribution

There is a general progression to longer periods at cooler temperatures in the data of Figure 11 and, as Figure 13 illustrates, nearly all of the redder stars have longer periods than their bluer companions. The dashed line in the figure represents the lower envelope of the period-period distribution. This trend toward longer periods at cooler temperatures is consistent with the various models mentioned above, but there is a wide range in the individual gradients, including several pairs with negative slopes.

If indeed stars of the same mass spin down uniformly with age, the rotation periods of the two (presumably coeval) components of equal mass binaries should be the same, within the uncertainties. There are 16 active CPM pairs in Table 2 with (g-K) colors within 0.5 magnitudes of one another and periods longer than 5.0 days; over such a short range in color, the two components can be expected to have almost the same mass and so should have nearly the same period. Figure 14 shows that although there is an apparent correlation between the periods of the A and B components, there is also considerable scatter. (There is also a small bias toward longer periods for the red component compared to the blue one, as expected.) The Pearson correlation coefficient of the x and y values of the points in Figure 14 is r = 0.80. In 1000 tries of random pairings of the 32 stars, the correlation coefficient never exceeded this value, indicating a confidence level in excess of 99.9%. The RMS difference between the red components and blue components is 6.2 days, much larger than the typical measurement uncertainty in the periods (see Table 2). So while the periods

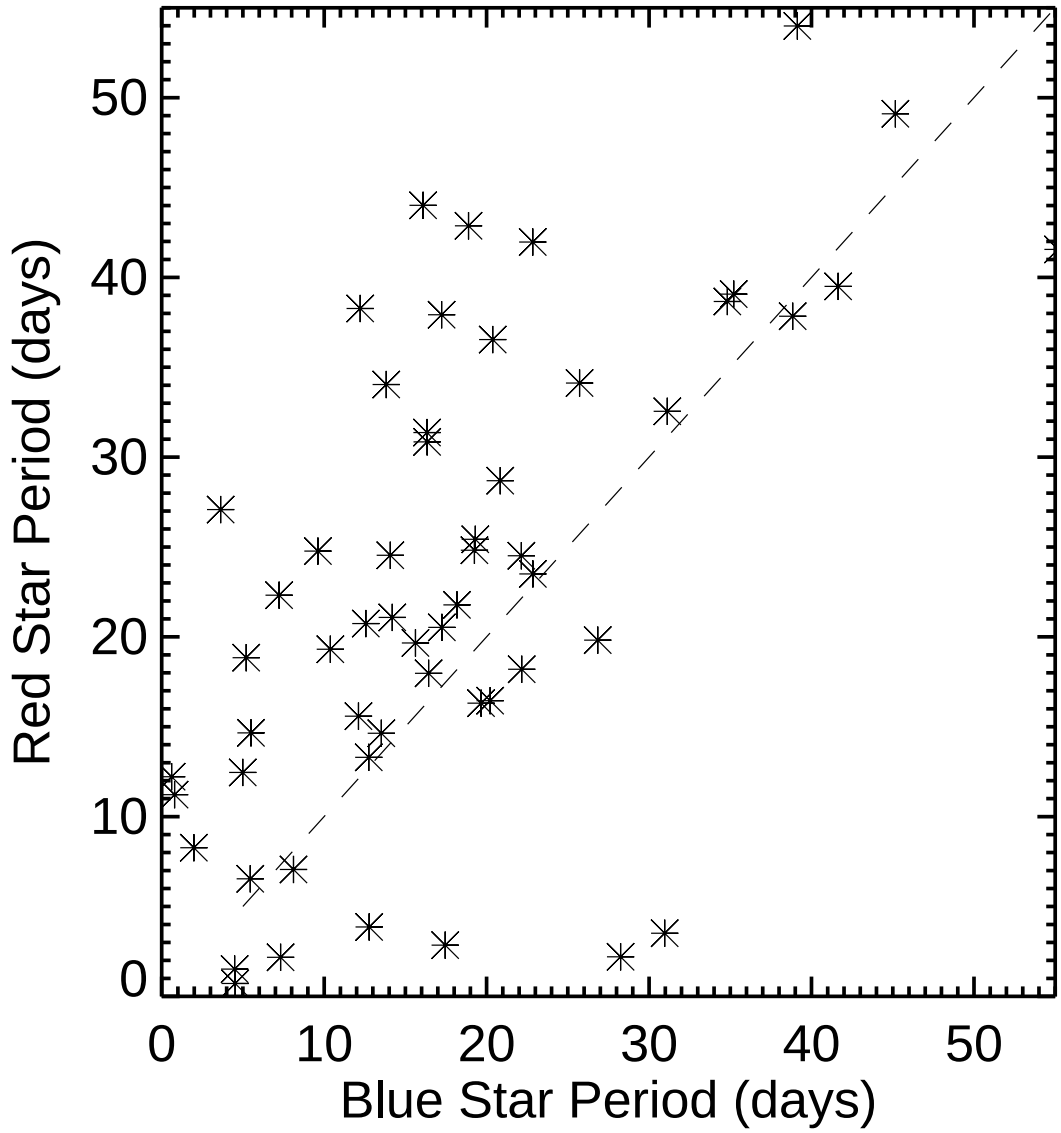

Fig. 13.— Periods of the blue member of each pair vs the red component period. The solid line in the figure has a slope of one. Nearly all of the red components have longer periods than their blue companions.

of the red and blue components are correlated, in some cases, there are large differences in their periods

5.2. The age-period-color relation

Barnes (2007); Mamajek & Hillenbrand (2008); Angus, et al. (2015) and others have proposed that rotation periods vs mass (i.e., effective temperatures or colors) and vs ages are separable functions, $P = f(T_{eff})g(A)$. Barnes assumed the Skumanich (1972) power-law relation for $g(A)$. Mamajek & Hillenbrand (2008) and Angus, et al. (2015) found slightly different power values for the age factor, $P \propto A^{0.56}$ and $P \propto A^{0.55}$ respectively. All three of these groups derived a power law of (B-V) color index to represent effective temperature (or main sequence mass). More recently, Barnes (2010) developed a more detailed theoretical formulation of the age-period-color relation. His isochrones (period-color relations at fixed age) for 4.57 Gyr and 600 Myr stars are also shown in Figure 12. The dashed green lines are from Barnes (2010) and the purple dotted lines are from Angus, et al. (2015). The upper two lines are the 4.57 Gyr isochrones. The central dotted purple line represents an Angus, et al. 2.5 Gyr isochrone. The Barnes (2010) isochrones are taken from a tabular version of his Figure 11 which he kindly provided.

Using the Barnes (2010) procedure, I calculated the ages of the "best" selection of systems from the catalog. As Figure 12 shows, the gradients of the period-color curves of the hotter stars with $(B - V) > 0.6$ are expected to be very steep, and the short-period stars with P less than 5 days are either very young or possibly they have tidally-locked close companions; I excluded both groups. The derived ages are shown in Figure 15; there is no obvious correlation between the calculated ages of the components.

So although Figures 11 and 12 support the gyrochronology concept in a general sort of

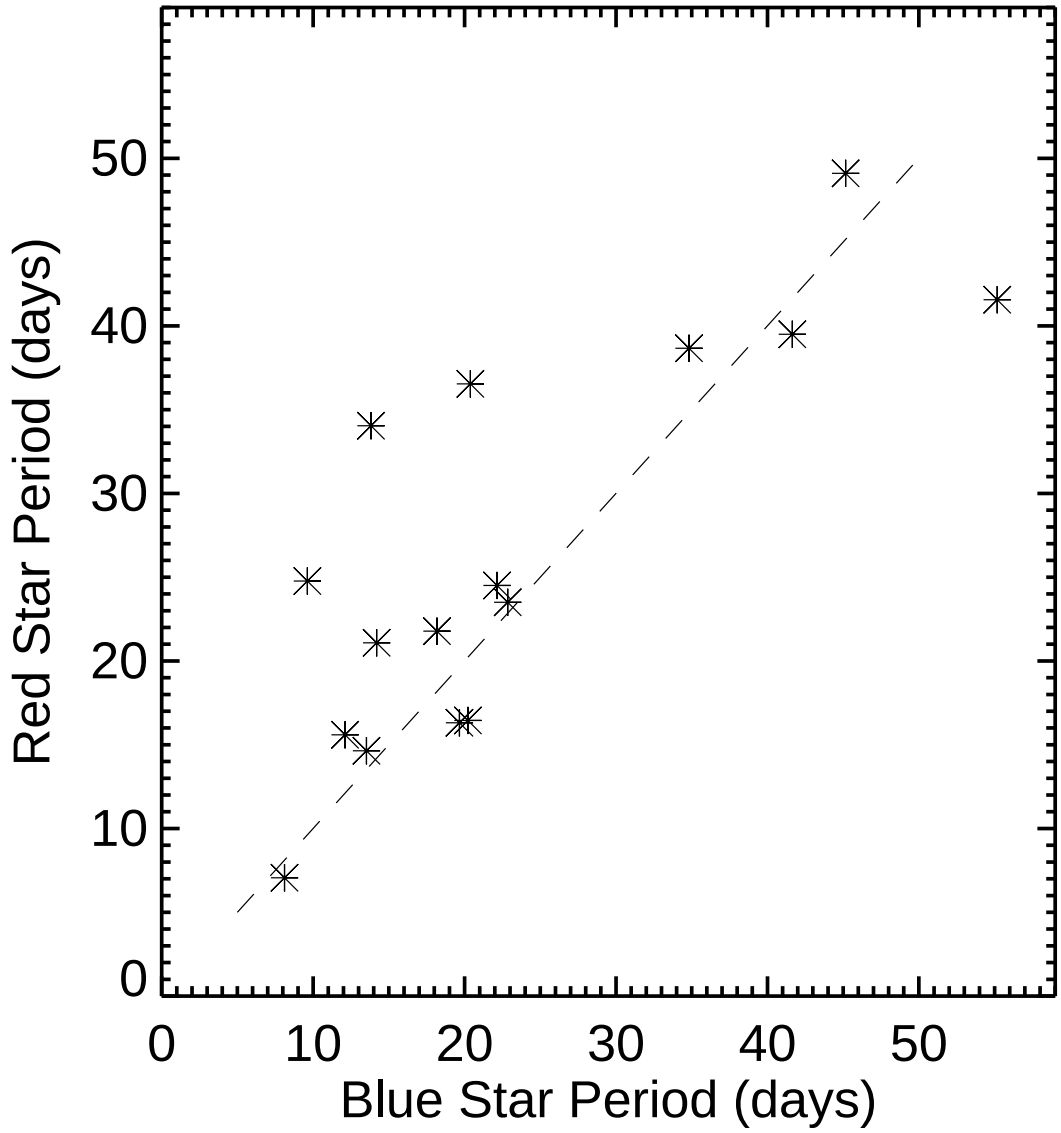

Fig. 14.— Periods of the 2 components of pairs with (g-K) color differences less than 0.5 magnitudes. For reference, the line has a slope of one.

way, the heterogeneous slopes of the lines connecting the binary pairs are not consistent with a simple age-period-color relation.

5.3. The upper envelope of the period-color distribution

Figures 11 and 12 show that near the solar color, there are relatively few stars with measureable rotation periods longer than the Sun's period. Furthermore, since the lines connecting the binary components represent lines of equal age, then the figure as a whole also suggests that there may be no more than a few *active* stars older than the Sun, even though the Sun is only about half the age of the disk. This same upper envelope of rotation periods can be seen in a much larger sample of Kepler stars in Figure 1 of McQuillan, et al. (2014).

Recently van Saders, et al. (2016) claimed that past the solar age, weakened magnetic braking results in a decline, or cessation in the rate of slowing of surface rotation. In their analysis, they made use of asteroseismic ages. But at least in the F, G and early K spectral types, stellar activity declines as the star slows down (see Figure 9), and older stars (i.e., those with longer periods) might not be sufficiently active for their rotation periods to be measurable. Furthermore, the wide binary star systems in this sample are weakly bound or not bound at all; any older pairs may drift far enough apart to be unrecognizable as common proper motion stars. So the apparent lack of binary systems with longer periods in Figures 11 and 12 cannot be used to address the van Saders, et al. (2016) hypothesis. That is to say, if there are stars at, say the solar color, with longer periods than the Sun, such stars would likely not show up in this sample.

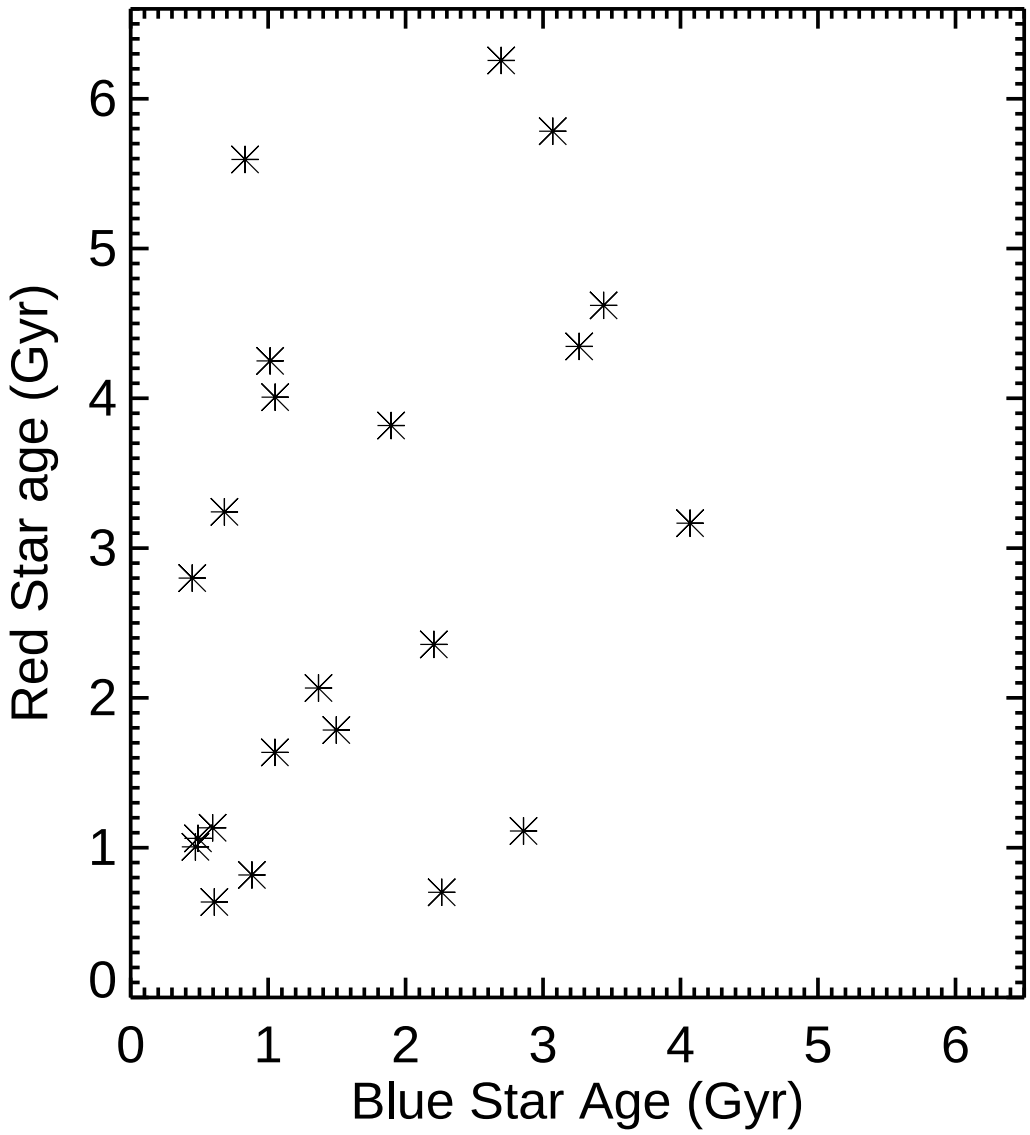

Fig. 15.— Ages of the 2 components of the "best" binaries (those with $(B-V) > 0.6$ and $P > 5$ days) calculated using the Barnes (2010) procedure.

5.4. Gaps in the period distribution

Finally, beginning about $(g - K) = 3.0$, there is an apparent gap (visible most clearly in Figure 12) in the number of stars with intermediate periods around P = 20 days. In the present sample, there are also only a few stars with periods less than about 10 days.

Barnes (2007, 2010); Barnes & Kim (2010) have described two stages in the rotational evolution of solar-type stars. In the initial "C" stage, stars are rapidly rotating but with a range of initial velocities. They spin down for several hundred million years until they converge to the "I" sequence. By that time they have lost all "memory" of the initial conditions, and thereafter they spin down according to the Skumanich (1972) law.

The figures show that while there is a relatively uniform distribution of periods among the hotter stars, a gap is visible in Figure 12 (and somewhat less obviously in Figure 11) in the period distribution of the cooler stars at intermediate periods. The gap can be seen more clearly in Figure 16, which shows the period distribution of active stars projected to the periods they would have at (B-V) = 1.27 (about spectral type M0) relative to the period a star on the 2.5 Gyr isochrone would have at that same color. So for star i,

$$P_{M0}(i) = P(i)[\frac{P_{2.5}(M0)}{P_{2.5}(i)}], \tag{6}$$

where $P(i)$ is the measured period of star i, $P_{2.5}(i)$ is the period of a star on the 2.5 Gyr isochrone at the color of star i, and $P_{2.5}(M0)$ is the period of a star on the isochrone at spectral type M0. Both the "C/I" break near 10 days described by Barnes (2010) and the intermediate-period gap near 30 days are visible in this histogram.

McQuillan, et al. (2013) described **the 30 day** gap in their much larger sample of late K and early M stars from the Kepler database, and Newton, et al. (2016) saw a similar gap among mid-M stars in the Mearth survey. **Davenport (2016), after matching a subset of the McQuillan, et al. sample with the recent Gaia Collaboration (2016) data**

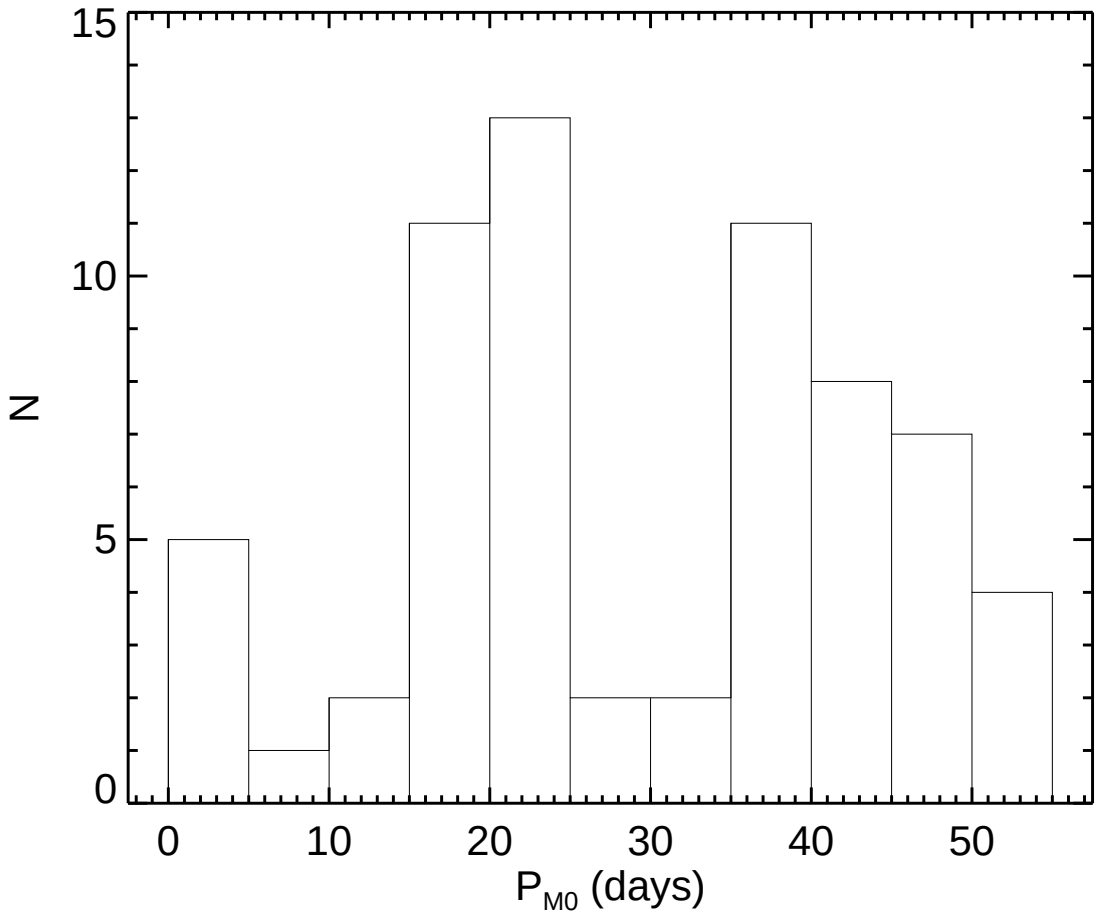

Fig. 16.— Histogram of stellar periods projected to the periods they would have at B-V = 1.27 (M0) relative to the period of a star along the 2.5 Gyr isochrone in Figure 12.

release 1, found evidence for a gap in the period distribution of bluer stars at periods near the 600 Myr rotational isochrone. He also traced the 600 Myr isochrone through the M-star gap, although that is not consistent with the appearance of Figure 12.

McQuillan, et al. (2013) **and Davenport (2016)** interpreted the gap as being the result of two distinct waves of star formation. However, if that were the case, one might expect the gap to extend through the entire range of colors (or masses). Newton, et al. (2016) interpreted the gap in their period data to a non-uniform rate of evolution, where after evolving slowly for several Gyr, stars enter a period of more rapid period evolution. On the other hand, Epstein & Pinsonneault (2014) have argued that even the long-term evolution of the lowest-mass stars is affected by the initial conditions.

As Figure 11 shows, there are several pairs of stars with quite different periods, one component being above the gap and the other below the gap. This suggests that the rotational evolution of the late K and early M stars proceeds in a non-uniform fashion, with some stars evolving in period more rapidly than others of the same mass.

6. Discussion

Figures 11 and 12 exhibit a considerable degree of complexity in the rotation period-age-color distribution of G, K and M dwarf stars. Some of the apparent complexity may be partly a consequence of the nature of the present sample of stars. There are several possible explanations:

1) Some of the pairs may not in fact be physical companions. As I described in Section 2, as many as 15% of the pairs selected on the basis of their proper motions could be accidental. Although eight of the original 102 pairs have photometric properties inconsistent

with being main-sequence stars at the same distance and have already been rejected (see Figure 8), perhaps a few more of the 56 pairs remaining in Figure 11 could also be unrelated to one another.

2) Some "pairs" are likely to be hierarchical triple systems consisting of a compact, tidally-locked pair and a much wider companion. I removed some of the stars with rapid variations earlier because they are probable close binary systems. But there could also be some longer-period stars whose periods are affected by tidal interactions as well.

3) The apparent starspot period may not be the true rotation period. For example if there are spots on opposite hemispheres, the true period could be twice the measured value. Wherever the autocorrelation function showed an obvious odd-even pattern of peak heights, I took the double period (as did McQuillan, et al. 2014). But there is also the possibility that even when alternate peaks are the same height, the actual rotation period could be twice the apparent period.

4) Because of differential rotation, the measured period over a time frame even as long as four years may not be the most representative period for a star's rotation period. In the Sun, the mean latitude of the spots, hence the solar rotation period (as measured by spots) varies over the solar cycle. Epstein & Pinsonneault (2014) discussed this matter at some length and considered that differential rotation is a primary limiting factor in determining the rotational ages of late-type stars.

5) Among the hotter stars in this sample, the steep gradients make the age calculation nearly indeterminate. This is true for the open cluster period-color diagrams which show a large range in period at fixed color at the blue end of the distribution. (See, e.g., Meibom, et al. (2011).) A few of the hotter stars may actually be pulsators, rather than spotted stars.

6) There may not be a single period-mass-age relation. Barnes & Kim (2010) have argued that after a few hundred million years, a star loses its "memory" of its initial rotation period and stars converge to a single period at a given age and temperature. But there may be other circumstances, such as companion stars or planets, to cause the gyro ages to diverge. In particular, the rotational evolution of otherwise apparently identical K and M stars could proceed in a non-uniform way, opening gaps or peaks in the period distribution at fixed color.

It is likely that at some level, all of these possibilities are operating. As stars evolve rotationally, their periods will gradually diverge from a mean period for the particular mass and age.

7. Summary

Using existing proper motion catalogs, I was able to identify 93 likely common proper motion pairs in the Kepler field. I was able to find reliable periods for about 2/3 of the stars, with 56 complete pairs with periods. The cooler (secondary) companions tend to have longer periods than the warmer (primary) components. The overall activity level of the cooler stars is at best only a weak function of rotation period. There are indications that either the rotation period evolution of the cooler stars proceeds at a non-uniform rate or some stars evolve more quickly than others of the same mass.

The great variety in the rotational properties of these stars and the small sample size make it impossible to derive a comprehensive period-age-color relation from the current data. Because of the large proper motion uncertainties in the existing catalogs, it was necessary to ignore the large majority of stars with small proper motions in searching for common proper motion pairs. However, future data releases from the Gaia mission (see

www.cosmos.esa.int/web/gaia/release) should make a dramatic change in the number of (wide) visual double stars available for evaluating the rotational history of the cool stars.

I want to thank Sydney Barnes for his help in preparing this paper and for providing me with rotational isochrones for Hyades and solar age stars. This research has been supported by the National Aeronautics and Space Administration under grant 13-ADAP13-0196. This research has made use of the MAST database at the Space Telescope Science Center and the VizieR catalogue access tool, CDS, Strasbourg, France. The original description of the VizieR service was published in A&AS, 143, 23. This publication makes use of the Two-Micron All Sky Survey which is a joint project of the University of Massachusetts and the Infrared Processing and Analysis Center/California Institute of Technology, funded by NASA and the NSF. I want to acknowledge the constructive comments of an anonymous reviewer that led to a number of improvements to the final version.

Facilities: Kepler

REFERENCES

Angus, R., Aigrain, S., Foreman-Mackey, D., & McQuillan, A., 2015, MNRAS, 450, 1787

Barnes, S.A., 2007, ApJ, 669, 1167

Barnes, S.A., 2010, ApJ, 722, 222

Barnes, S.A. & Kim, Y.-C., 2010, ApJ, 721, 675

Barnes, S.A., Weingrill, J., Fritzewski, D., Strassmeier, K.G., & Platais, I., 2016, Ap.J., 823, 16

Basri, G., Walkowicz, L.M., & Reimers, A., 2013, ApJ, 769, 37

Bedin, L.R., Salaris, M., Anderson, J., Cassisi, S., Milone, A.P., Piotto, G., King, I.R., & Bergeron, P., 2015, MNRAS, 448, 1779

Borucki, W.J., Koch, D.G., Basri, G., Batalha, N., Boss, A., Brown, T.M., Caldwell, D., Christensen-Dalsgaard, J., Cochran, W.D., DeVore, E., & 52 coauthors, 2011, ApJ, 728, 117

Connelly, J.N., Bizzarro, M., Krot, A.N., Nordlund, Å, Wielandt, D., & Ivanova, M.A., 2012, Science, 338, 651

Davenport, J.R.A., 2016, ArXiv e-prints, arXiv:1610.085653

Deacon, N. R., Kraus, A. L., Mann, A. W., Magnier, E. A., Chambers, K. C., Wainscoat, R. J., Tonry, J. L., Kaiser, N., Waters, C., Flewelling, H., & 2 coauthors, 2016, MNRAS, 455, 4212

Donahue, R.A., 1998, A.S.P. Conf. Ser., 154, "The Tenth Cambridge Conference on Cool Stars, Stellar Systems and the Sun," Eds., R.A. Donahue & J.A. Bookbinder

Epstein, C.R. & Pinsonneault, M.H., 2014, ApJ, 780, 159

Gaia Collaboration, 2016, ArXiv e-prints, arXiv:1609.04153

Høg, E., Fabricius, C., Makarov, V.V., Urban, S., Corbin, T., Wycoff, G., Bastian, U., Schwekendiek, P., & Wicenec, A., 2000, A&A, 357, 367

Huber, D., Aguirre, V.S., Matthews, J.M., Pinsonneault, M.H., Gaidos, E., Garcia, R.A., Hekker, S., Mathur, S., Mosser, B., Torres, G., Bastien, F.A., & 11 coauthors, 2014, ApJS, 211, 2

Kawaler, S.D., 1988, ApJ, 333, 236

Kirk, B., Conroy, K., Prša, A., Abdul-Mosih, M., Kochoska, A., Matijevič, G., Hambleton, K., Barclay, T., Bloemen, S., Boyajian, T., & 40 coauthors, 2016, AJ, 151, 68

Kraus, A.L., & Hillenbrand, L.A., 2007, AJ, 134, 2340

Mamajek, E.E. & Hillenbrand, L.A., 2008, ApJ, 687, 1264

McQuillan, A., Aigrain, S., & Mazeh, T., 2013, MNRAS, 432, 1203

McQuillan, A., Aigrain, S., & Mazeh, T., 2014, ApJS, 211, 24

Meibom, S., Barnes, S.A., Latham, D.W., Batalha, N., Borucki, W.J., Koch, D.G., Basri, G., Walkowicz, L.M., Janes, K.A., Jenkins, J., & 10 coauthors, 2011, ApJ, 733, 9

Meibom, S., Barnes, S.A., Platais, I., Gilliland, R.L., Latham, D.W., & Mathieu, R.D., 2015, Nature, 517, 589

Monet, D., Levine, S., Canzian, B., Ables, H., Bird, A., Dahn, C., Guetter, H., Harris, H., Henden, A., Leggett, S., & 19 coauthors, 2003, AJ, 125, 984

Newton, E.R., Irwin, J., Charbonneau, D., Berta-Thompson, Z.K., Dittmann, J.A., & West, A.A., ApJ, 821, 181

Noyes, R.W., Hartmann, L.W., Baliunas, S.L., Duncan, D.K., & Vaughan, A.H., 1984, ApJ, 279, 763

Reinhold, T., Reimers, A., & Basri, G., 2013, A&A, 560, 19

Roeser, S., Demleitner, M., & Schilbach, E., 2010, AJ, 139, 2440

Skumanich, A., 1972, ApJ, 171, 565

van Saders, J.L., Ceillier, T., Metcalfe, T.S., Silva, Aguirre, V., Pinsonneault, M.H., García, R.A., Mathur, S., & Davies, G.R., 2016, Nature, 529, 181

Yuan, H.B., Liu, X.W., & Xiang, M.S., 2013, MNRAS, 430, 2188

Zacharias, N., Finch, C.T., Girard, T.M., Henden, A., Bartlett, J.L., Monet, D.G., & Zacharias, M.I, 2013, AJ, 145, 44

Zacharias N., Finch C., Subasavage J., Bredthauer G., Crockett C., Divittorio M., Furguson E., Harris F., Harris H., Henden A., & 7 coauthors, 2015, AJ, 150, 101

This manuscript was prepared with the AAS LaTeX macros v5.2.